Manuscript final draft for submission to Journal of Volcanology and Geothermal Research

January 2020

PREPRINT: a doi will be provided in due course to the final peer-reviewed article

Comments are welcome by contacting the corresponding author directly

Pleistocene - Holocene volcanism at the Karkar geothermal prospect, Armenia

Khachatur Meliksetian[1], Iain Neill[2*], Dan N. Barfod[3], Eilidh J.M. Milne[2], Emma C. Waters[4], Gevorg Navasardyan[1], Edmond Grigoryan[1], Valerie Olive[5], Nicholas Odling[6], Arkady Karakhanian[1†]

[1]Institute of Geological Sciences, National Academy of Sciences, 24a Marshal Baghramyan Avenue, 0019, Yerevan, Armenia.
[2]School of Geographical and Earth Sciences, University of Glasgow, Gregory Building, Lilybank Gardens, Glasgow, G12 8QQ, Scotland.
[3]NEIF Argon Isotope Facility, Scottish Universities Environmental Research Centre, Rankine Avenue, Scottish Enterprise Technology Park, East Kilbride, G75 0QF, Scotland.
[4]School of Earth and Environmental Sciences, University of Manchester, Williamson Building, Oxford Road, Manchester, M13 9PL, England.
[5]Scottish Universities Environmental Research Centre, Rankine Avenue, Scottish Enterprise Technology Park, East Kilbride, G75 0QF, UK.
[6]School of GeoSciences, Grant Institute, University of Edinburgh, Kings Buildings, James Hutton Road, Edinburgh, EH9 3FE, Scotland.
[†]Deceased.
[*]Corresponding author. E-mail: iain.neill@glasgow.ac.uk; Phone: +44 1413 305477.

Abstract

Pleistocene to Holocene volcanic centres north of the Bitlis-Zagros suture in Turkey, Iran, Armenia and Georgia represent both volcanic hazards and potential or actual geothermal energy resources. Such challenges and opportunities cannot be fully quantified without understanding these volcanoes' petrogenesis, geochronology and magmatic, tectonic or other eruption triggers. We discuss the age and igneous geology of the Karkar monogenetic volcanic field in Syunik, SE Armenia. The ~30 km^2 field is beside the location of Armenia's only geothermal energy test drilling site. Eruptions of fissure-fed trachybasaltic andesite to trachyandesite occurred on a trans-tensional pull-apart segment of the Pambak-Sevan-Syunik Fault and have previously been interpreted to be of Holocene age. We conducted high-resolution duplicate $^{40}Ar/^{39}Ar$ dating of 7 groundmass separates, providing composite plateau or inverse isochron ages ranging from 6 ± 3 ka to 332 ± 9 ka (2σ). Each lava flow displays petrographic and geochemical patterns consistent with melting of subduction-modified lithospheric mantle and crystal fractionation involving ol, sp, opx and cpx, amp and plg. Some crystal-scale zoning was observed, implying recharge prior to eruption, and a preliminary estimate of cpx crystallisation pressures indicates storage in the mid- to upper crust, which may be of relevance for geothermal developments. These data indicate that volcanic activity in Syunik and elsewhere in Armenia overlapped with human occupation and that the presence of a substantive heat source for geothermal energy and a lava inundation hazard for local infrastructure should be further considered. Additional geophysical monitoring of the Pambak-Sevan-Syunik Fault is merited, along with detailed determination of the depths of magma storage both here and also at Porak volcano 40 km north of Karkar.

Keywords

Armenia; $^{40}Ar/^{39}Ar$ geochronology; Geochemistry; Geothermal Energy; Monogenetic Volcanism; Hazards

Highlights

- Monogenetic volcanism close to new geothermal energy development in SE Armenian Uplands
- Last eruptions during the Holocene based on $^{40}Ar/^{39}Ar$ geochronology and archaeology
- Magmas sourced from sub-continental mantle lithosphere followed by fractionation in mid-upper crust
- Further dating and identification of heat sources important for geothermal development

- Volcanism still poses a hazard in this area and geophysical monitoring is recommended

1. Introduction

Armenia (pop. ~3.0 million) is a landlocked nation in the South Caucasus. As a former Soviet state, with difficult political relations with neighbours Turkey and Azerbaijan, and closed borders, Armenia's energy needs are heavily dependent both on Russian and Iranian hydrocarbon supplies and on the Metsamor nuclear facility located 30 km west of the capital city, Yerevan (Fig. 1). Recently, the Armenian government have increased investment in renewable energy prospects, including hydropower, wind, solar and geothermal energy. In 2008-2015 the World Bank supported detailed geological, geophysical investigations within the Karkar plateau followed by drilling of two test wells that began in 2016 at the Karkar geothermal site. The site lies in Syunik Province in the remote SE of the country (Fig. 1). The Karkar site was recognised as promising based on earlier studies from a well drilled in 1988 (Fig. 2; Gilliland et al., 2018; Georisk, 2012; White et al., 2015). The site is on a plateau around 3,000 m a.s.l., formed largely from late Cenozoic lava flows and intrusions, and cut by the Syunik branch of the Pambak-Sevan-Syunik (PSSF) fault system (Karakhanian et al., 1997; Meliksetian, 2013).

Armenia has an extensive history of Late Cenozoic volcanism, related to the Arabia-Eurasia collision. However, compared to other active or potentially active volcanic areas globally, few modern and precise geochronological and petrogenetic studies have been carried out (Neill et al., 2013, 2015; Sugden et al., 2019). There are some permanent and temporary geophysical monitoring networks which may help monitor the movement of magma at depth within the crust (Sargsyan et al., 2017), but just two installations are reasonably near, at 25 and 50 km, to the Karkar site. Several volcanic uplands in Armenia are likely to have experienced Holocene eruptions, but most records depend on interpretations of ancient manuscripts, inscriptions and petroglyphs, ^{14}C dating of archaeological sites and on post-glacial geomorphology (Karakhanian et al., 2002). To our knowledge none of the youngest, potentially Holocene, volcanic centres have peer-reviewed data for the depth of magma storage, their eruption triggers or radiometric determinations of their precise age, though a range of unpublished radiometric and cosmogenic dates are emerging. There is an urgent need to fill this knowledge gap around volcanic activity, considering both volcanic hazards and the country's potential future energy investments. Therefore, this paper's primary objective is to document the age and petrogenesis of the youngest magmatism in the Karkar monogenetic volcanic field, given its importance as Armenia's first geothermal test drilling site. We will use: (1) high-resolution $^{40}Ar/^{39}Ar$ dating to further assess evidence for Holocene volcanic activity at Karkar; (2) petrography and geochemistry to consider the petrogenesis of the erupted lavas and compare them to other recent magmatism across Armenia; and (3) qualitative assessment of the magmatic history and local tectonics to guide further research and recommendations for exploitation of geothermal energy.

2. Geological Background

2.1. Geology of Armenia

Armenia is landlocked in the South Caucasus mountains between Iran, Georgia, Azerbaijan and Turkey (Fig. 1), and consists of two crustal domains. To the north and north-east are assemblages of mostly island arc-related igneous rocks formed during closure of the northern branch of the Neo-Tethys Ocean during the Mesozoic (Galoyan, et al., 2007, Mederer et al. 2013; Rolland et al. 2017). In the south lies the South Armenian Block (SAB), which is poorly exposed beneath Cenozoic volcanic and sedimentary rocks. The SAB is considered to represent a microcontinental fragment of Proterozoic to Palaeozoic age that is assumed to have detached from Gondwanaland during the formation of Neo-Tethys (Sosson et al. 2010). Between these two domains is a structurally complex zone of ophiolitic fragments of mostly Jurassic to Cretaceous age (Galoyan et al. 2007, Sosson et al. 2010). Eocene intrusive rocks across much of Armenia are a product of back-arc extension during subduction of the southern branch of Neo-Tethys beneath Turkey and Iran (Sahakyan et al. 2016). Armenia has experienced late Cenozoic transpressional tectonics due to the ongoing Arabia-Eurasia collision and is today crossed by the right-lateral Pambak-Sevan-Syunik Fault (PSSF), which cuts through Lake Sevan and has several branches extending for ~400 kilometres NW-SE and N-S through the country, exploiting the older suture. There is modern and historical evidence for centennial-millennial earthquakes $\geq M_w$ 7.0, including the 1988 Spitak quake that killed 25,000 over the north of Armenia (Karakhanian et al. 2004). Extensive Late Cenozoic collisional magmatism is spatially related to zones of extension triggered by fault curvature, local pull-apart structures or interactions between several fault systems (Karakhanian et al. 2002; Neill et al. 2013). Recent geochemical analyses demonstrate a subduction-

modified sub-continental lithospheric source (Sugden et al. 2019). Magmatism largely post-dates break-off of one or more Neo-Tethyan slabs and therefore is likely to be driven by combinations of long-lived mantle upwelling due to break-off, sub-lithospheric convection and lithospheric thinning, and petrological considerations such as melting due to lithospheric mantle crossing the amphibole peridotite solidus at depths of ~70-90 km within the lithosphere (Neill et al. 2015; Sugden et al. 2019).

There are hundreds of Quaternary vents and fissures built up into ridges and plateaux related to faults across Armenia. These include the Javakheti Ridge which extends into Georgia, related to extensional tectonics north of the PSSF (Neill et al. 2013); the Gegham Ridge in Gegharkunik Province which directly overlies the Garni Fault; (Karakhanian et al. 2002); and Porak volcano and the Karkar monogenetic volcanic field in Syunik Province in the SE. The last two of these lies along the Syunik branch of the PSSF that extends directly N-S from Lake Sevan (Karakhanian et al. 1997; 2002). Much larger stratovolcanoes and related monogenetic cones have also been constructed during the Late Cenozoic, including Aragats (Armenia's highest peak at 4090 m), Arailer just to the east of Aragats, and Tskhouk and Ishkanasar just south of Karkar (Gevorgyan et al. 2018; Meliksetian 2013). There are also some isolated monogenetic centres such as Vayots Sar and Smbatassar which may be spatially related to unmapped faults (Fig. 1).

An estimate of future potential for volcanic activity is far from complete, in part because published peer-reviewed radiometric dating of Holocene volcanism is patchy. Two volcanic cones south of Karkar provided near-zero $^{40}Ar/^{30}Ar$ ages which might be interpreted as Holocene (Ollivier et al. 2010). A further geomorphologically very fresh cone suspected to be of Holocene age, Smbatassar, 55 km west of Karkar, did not produce detectable radiogenic Ar (Koppers and Miggins personal communication 2018; Karakhanian et al. 2002). Aside from the new $^{40}Ar/^{39}Ar$ data reported here there is an $^{40}Ar/^{39}Ar$ date of 3.7 ± 4.2 ka (2σ), yet to be peer-reviewed, from a flow at the Porak volcano some 40 km north of Karkar on the same segment of the PSSF (Meliksetian et al. 2018). Otherwise, archaeological and geomorphological evidence has been used several times to argue for Holocene volcanic activity by Karakhanian et al. (1997; 2002) and Karakhanian and Abgaryan (2004). They document at least two eruptions at Porak and two or more at Karkar during the Holocene, with evidence including: (1) fresh volcanic cones and flows which have no evidence of glacial erosion; (2) manuscript records, cuneiform inscriptions and rock carvings which have been interpreted to depict volcanic activity, often coinciding with strong earthquakes and periods of conflict or social upheaval and (3) ^{14}C dating of archaeological sites deemed to be affected by later volcanic activity. Finally, some permanent and temporary passive seismic stations near Gegham Ridge (Fig. 1) have begun picking seismic swarms of volcano-tectonic origin, consistent with an active magma chamber at ~20 km depth (Sargsyan et al. 2017). In summary, there is now a pressing need for corroboration of Holocene volcanic activity, both from a volcanic hazard perspective, and in preparation for sustainable exploitation of geothermal sources, especially given high heat flow and magmatic fluid sources reported from thermal springs across Armenia (Meliksetian et al. 2017).

Figure 1. A map of Armenia in the South Caucasus showing the locations of major volcanoes or volcanic fields, faults, and towns mentioned in this text. Background relief map extracted from GeoMapApp v3.6.10 (http://geomapapp.org; Ryan et al. 2009).

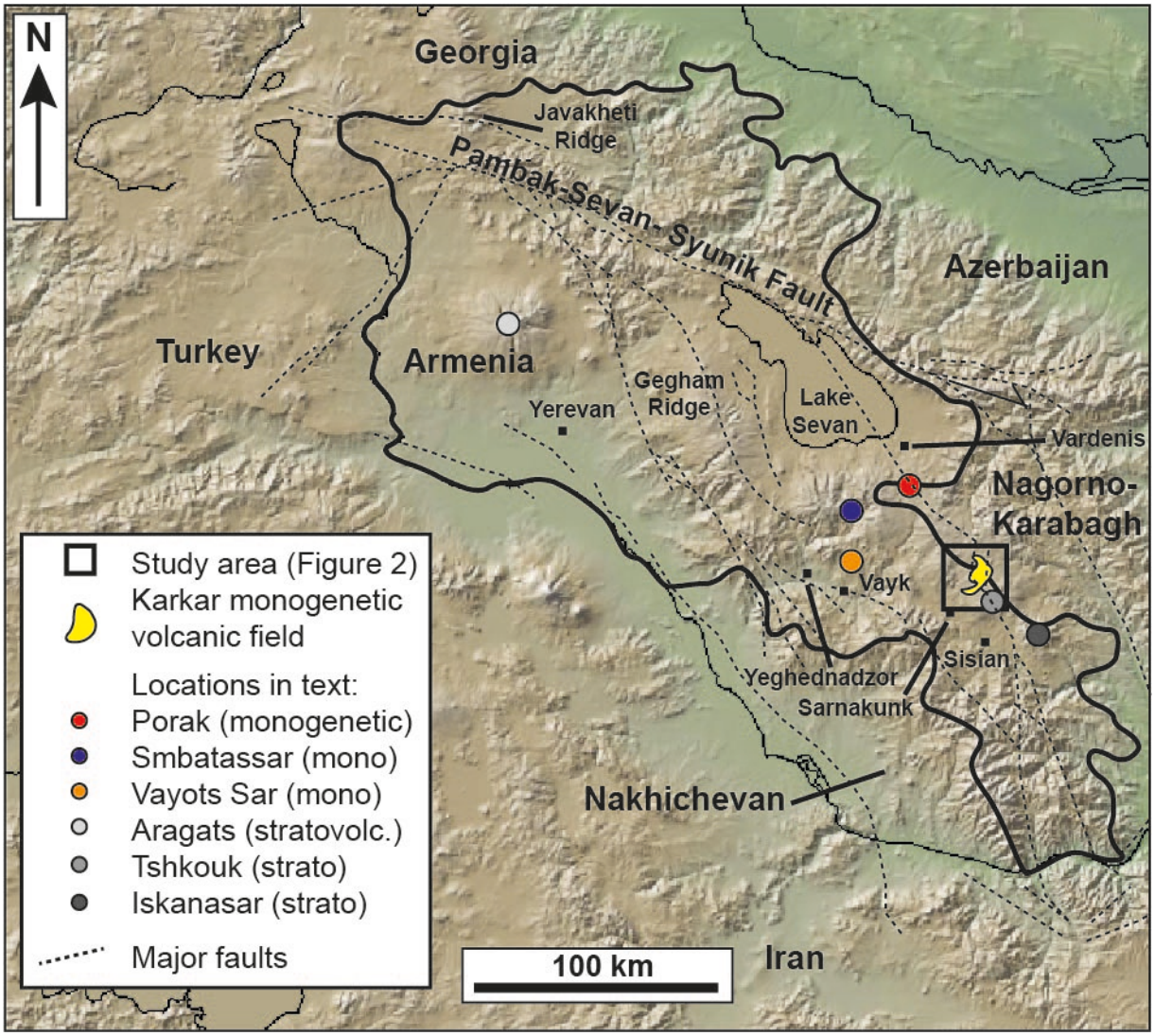

2.2. Introduction to the Karkar monogenetic volcanic field

The Karkar monogenetic volcanic field in Syunik Province (Fig. 2) begins immediately south of the location of new test boreholes spud in 2016, B1 and B2, for the exploration of geothermal resources. These boreholes reached depths of approximately 1600 metres, and superseded a nearby 1988 borehole called N-4, which reached 1000 metres. Figure 3 contains a cross section of the Karkar field along with a summary of borehole records based on Gilliland et al. (2018). These boreholes give us our best indication of the sub-surface geology beneath the most recent lava flows in this study.

The youngest volcanic rocks at Karkar are fissure-fed cones and lavas that cover ~30 km^2 and lie northwest of two much larger polygenetic stratovolcanoes, Tskhouk and Ishkanasar, which were active during the Pleistocene (Ollivier et al. 2010; Meliksetian 2013; Sugden et al. 2019). N-S-trending transtensional faults cut the area, and carbon-14 dates indicate fault motion has continued to the last couple of millennia (Karakhanian et al. 2002; Neill and Dunbar, unpublished data 2018). Karakhanian et al. (2002) interpreted the faults to define a small pull-apart basin on a step-over between segments of the transpressive Syunik Fault. The youngest lavas overlie a subdued landscape of glacially eroded, presumed Pleistocene volcanic cones and lavas, although in borehole logs there are reports of tuff and alluvium (Gilliland et al. 2018). Though the tuff is a plausible identification, given the proximity of Tskhouk and Ishkanasar stratovolcanoes, we viewed the borehole chippings in 2016 and considered much of the material as lava which had experienced extensive hydrothermal alteration, resulting in a yellow-brown, clay-rich texture with partially corroded phenocrysts. These materials reach a depth of almost 1000 m in both wells B1 and B2 and are cut by a body of quartz monzonite encountered in well B2 at 155-241 m depth. GeoRisk (2012) argued the monzonite was part of a series of shallow syenite domes or plugs, but they have never been precisely dated and are currently recorded as ‘Neogene-Quaternary’ (Fig. 3). Much of the local area is further underlain by an alkaline granitoid body or bodies collectively called the Dalidagh intrusion (GeoRisk, 2012). The Dalidagh body is

presumed to have an Eocene phase based on K-Ar dating and comparison with Early Eocene-Early Miocene Meghri and Bargushat plutons dated by K-Ar and U-Pb methods (Ghukasyan & Meliksetian, 1965, Moritz et al, 2016). These plutons are exposed ~50 km south of Karkar along tectonic strike. Small intrusive exposures across the wider area suggest further phases including those of speculated early Miocene, early Oligocene and possibly younger ages, but these are also largely based on petrographic comparison with other units (GeoRisk, 2012). Wells B1 and B2 record that the country rock hosting these magmatic bodies forms part of the suture between the SAB and the Eurasian margin (Sosson et al. 2010). Rock types include dolomitic marble, greywacke, quartzite and serpentinite to the base of the wells, sometimes associated with significant permeability. A lack of nearby seismic stations means few recent earthquakes have been recorded near Karkar, however GPS stations record dextral fault motion of around 0.5 mm/yr on the Syunik branch of the PSSF (Karakhanian et al. 2013) raising the possibility that some deformation is taken up by aseismic slip or creep in weak lithologies such as the aforementioned serpentinite.

Figure 2. a) False colour image of the Karkar monogenetic field overlain with sample locations (squares), the youngest identified eruption sites (X) and weighted mean plateau ages. Image obtained using Copernicus Sentinel 2 L1-C data (19-10-2018), retrieved from https://apps.sentinel-hub.com (19-2-2019), processed by the European Space Agency. b) Geological map of the Karkar monogenetic volcanic field, as interpreted by the Institute for Geological Sciences of the National Academy of Sciences in Armenia, and the approximate location of the cross-section line for Figure 3. Key for the map units: 1: Holocene basaltic trachyandesites. 1a = 1st generation lava flow; 1b = 2nd generation lava flow, etc. 2: Late Pliocene to Early Pleistocene basaltic trachyandesites, trachyandesites, trachytes, trachydacites, tuffs and volcanic breccias of the Tskhouk-Ishkanasar and Goris suites. 3: Late Pleistocene glacial and fluvioglacial deposits and moraines. 4: Late Pleistocene trachybasalts, basaltic trachyandesites, trachyandesites, basanites, phonotephrites. 5: Middle Pleistocene trachybasalts, basaltic trachyandesites, basanites and phonotephrites. 7: Early Pleistocene rhyolites, obsidian domes. 9: Monogenetic volcanic centres (mostly Late Pleistocene - Holocene). 10: Crater rim of Tskhouk stratovolcano. 11: Dome-shaped rhyolitic volcanoes and related extrusive rocks. 12: Active and supposed faults. 13: Lakes. 14: Rivers. Note the discrepancy between K16-2 and K16-3 which is discussed in the text; and that units 6 and 8 are not clearly identified within the map area and therefore not listed here: these would be parts of the Tskhouk-Ishkanasar and Goris suites where the specific volcanic source can be recognised.

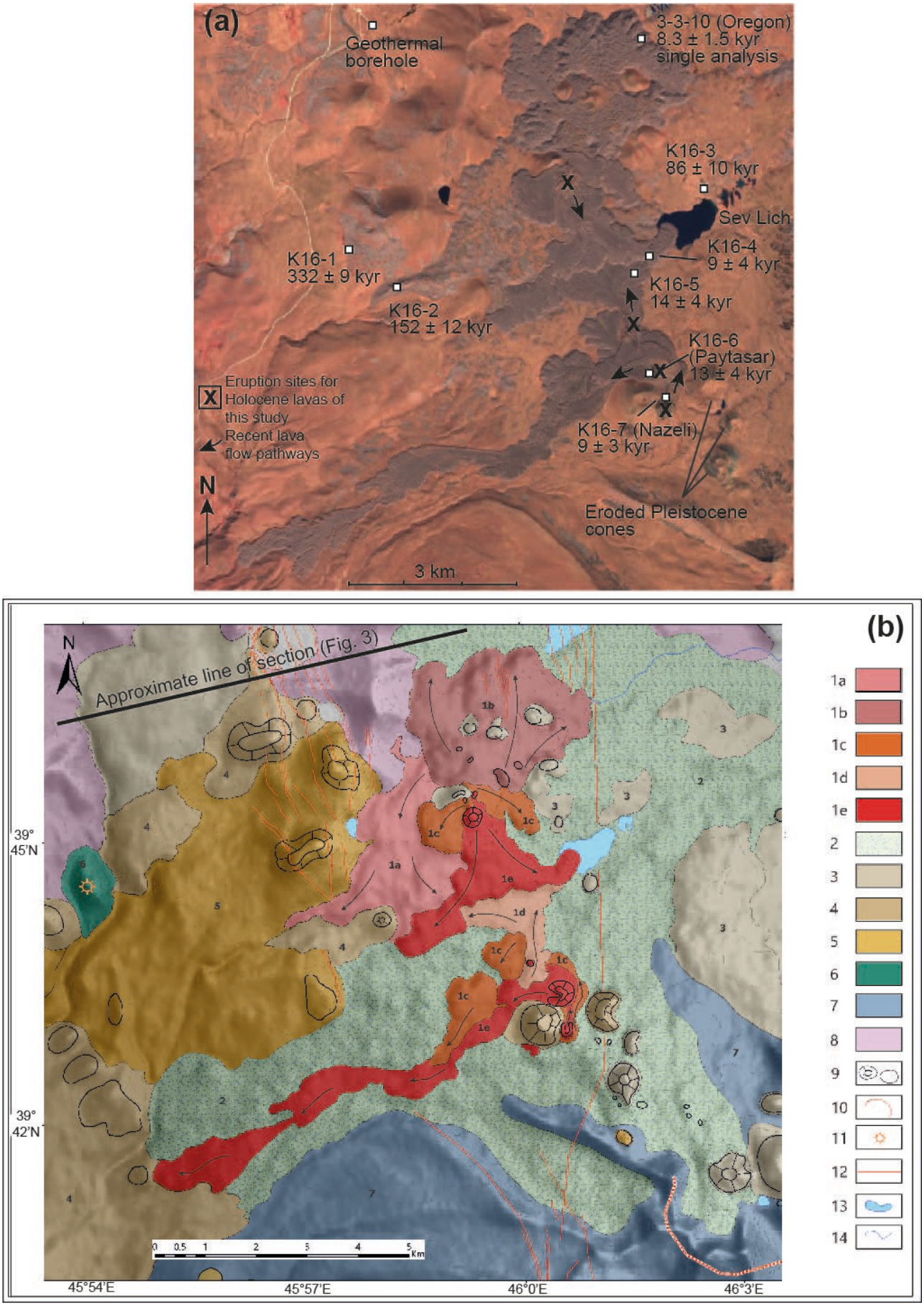

Prior to the drilling of wells B1 and B2, detailed magneto-telluric and gravity investigation was carried out (GeoRisk, 2012; White et al. 2015). White et al. (2015) proposed that the geothermal resource was based not on the

most recent volcanic materials but on the shallow quartz monzonite intrusion(s). It is vital that this body be assigned a precise absolute age in the future. However, Gilliland et al.'s (2018) updated model suggested a deeper, unknown heat source. White et al. (2015) concluded that the geothermal waters were largely meteoric in origin, fed through faults and eventually returned to the surface via hot springs. The 1980's N-4 borehole cut into the uppermost parts of the Dalidagh body, encountering temperatures of nearly 100°C at a depth of 1 km (Georisk, 2012). The later B1 borehole recorded 116°C at 1460 m (Gilliland et al. 2018). A modest injectivity of 7 t hr^{-1} bar^{-1} was recorded in 2016 and a fluid flow of 80 l min^{-1}. The B2 borehole recorded 124°C at 1600 m, rising to 135 °C by the end of testing, with an injectivity of 0.7 t hr^{-1} bar^{-1}. A noted >250 m difference in static water level between the two boreholes was explained by the two boreholes being separated by one of several faults which have probably caused reservoir compartmentalisation (Gilliland et al. 2018). The final conclusions of Gilliland et al. (2018) were that the main permeable depths in the existing B1 and B2 wells were potentially suitable for district heating use, but that the hotter deep part of the wells passed through largely impermeable material. By analogy with similar global examples, it was recommended the wells be extended to up to 3000 m depth beneath the surface for exploitation for electricity generation, where greater permeability was expected.

E-W Cross section model and schematic logs for the Karkar monogenetic field at the present day, as summarised and modified from Gilliland et al. (2018).

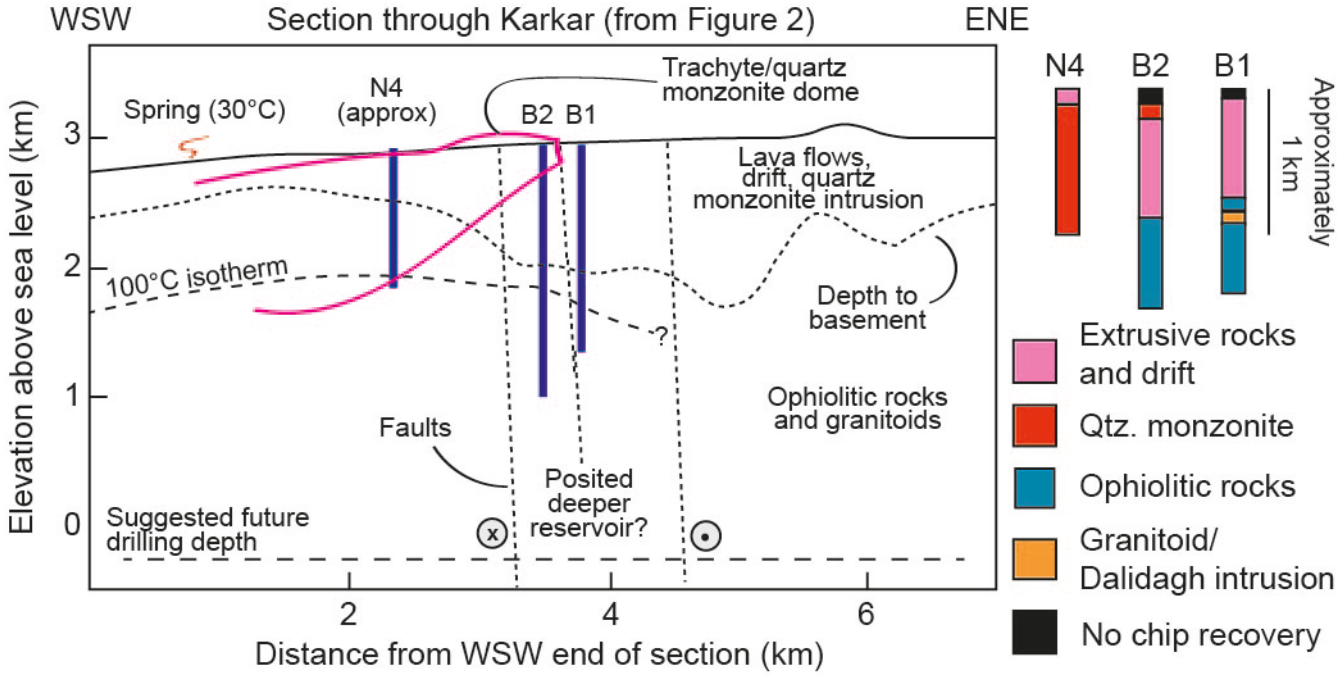

3. Fieldwork and petrography

We return to the question of the age and origin of the youngest monogenetic volcanic activity around Karkar. Seven lavas from immediately SE of the borehole locations were dated and geochemically analysed for this project, following a walk-over in summer 2016. Brief sample details are reported in Table 1. A single sample collected in 2015 from the most northerly of the Late Pleistocene – Holocene flows has been analysed separately at Oregon State University, providing a Holocene plateau age of 8.3 ± 1.5 ka (2σ, Balasanyan et al., 2018). This age, produced by Koppers and Miggins at the OSU geochronology lab, will be reported in full in a separate publication (Balasanyan et al., 2019, *submitted*). The recent lavas erupted from fissures with limited morphological expression (Fig. 4a) but demonstrate a clear N-S alignment of fissure sites (Figure 2a). In the south of the field area, fountaining behaviour built up cones of moderately scoriaceous agglomerate transiting to blocks with up to 50 m prominence (summits of Paytasar and Nazeli; Fig. 4b). Only weakly constrained by existing topography, the contemporary lavas have flowed between 1.5 and 8.5 km from source, the longest and most voluminous emitting from the summit of Paytasar (~77 x 10^6 m^3). Remote sensing reveals several hundred-metre long ogives intersected by linear cooling cracks, and there are occasional crease structures a few m deep visible on the ground (Fig. 4c). The lava flows range from weakly vesicular to slightly scoriaceous a'a to blocky type, with the majority of surfaces broken up into large dm- to m-scale blocks. Exposure is insufficient to appreciate more of the feeder system, but it is likely the magmas ascended in dyke-like fashion via existing fault planes or fractures. These formed in relation to the afore-mentioned pull-apart structure

between different branches of the PSSF. A total volume estimate for erupted Holocene lavas at Karkar is ~342 million m^3 (~0.3 km^3).

Figure 4. a) Overview of the Karkar field, taken from the lava flow of Nazeli volcano, showing typical landscapes and lava flows wrinkled into ogives. b) View of the Nazeli volcano (K16-7) showing a cone of breccia, blocks and bombs built up around the vent and the resulting lava flow. c) General morphology of the Karkar lava flows, showing a crease structure in flow K16-5. d) Cross-polarised light image of K16-2 (152 ± 12 ka) showing dominant sieve-textured plagioclase macrocrysts. e) Cross-polarised light image of K16-6 (13 ± 4 ka) with an amphibole-dominated phenocryst assemblage alongside clinopyroxene glomerocrysts. f) Cross-polarised light image of K16-6 showing clinopyroxene glomerocryst overgrown with amphibole and plagioclase.

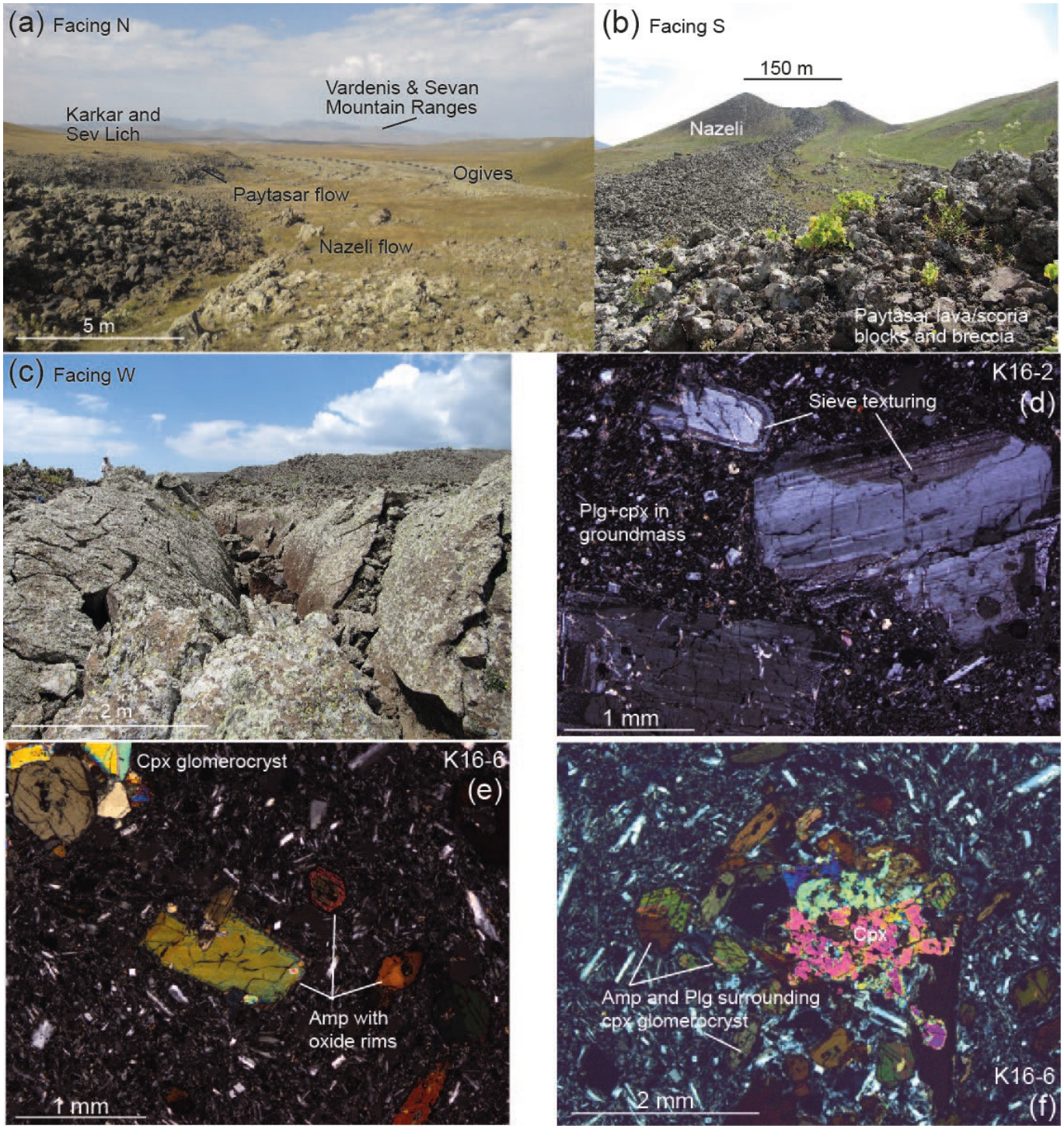

The majority of samples are fresh mafic to intermediate porphyritic lavas, mostly seriate-textured (Figs 4d-f). Lavas were preferentially sampled for comparatively low vesicularity (1-10 %; Table 1) but more vesicular and

scoriaceous materials are often found in the field, sometimes with white clay or calcite amygdales. The groundmass ranges from hypo- to holocrystalline in texture with ~0.25 mm grain size, excepting sample K16-7 which has up to 1 mm grain size in places. The groundmass is typically hyalopilitic, dominated by weakly-aligned plagioclase feldspar with subordinate clinopyroxene, oxides, apatite ± amphibole. Phenocrysts and glomerocrysts vary in abundance (5-20 %) and size (0.5 - 5 mm). In the youngest samples (K16-4 through 7), amphibole is the dominant phenocryst, with extensive oxide rims. Subordinate plagioclase and clinopyroxene phenocrysts are also present. The older samples (K16-1 through 3) contain varying proportions of plagioclase, clinopyroxene or orthopyroxene phenocrysts and only in K16-1 is a small proportion of amphibole present. Plagioclase is often optically zoned, and sieve textured. Ruby-coloured groundmass iddingsite may be evidence for the former presence of olivine. The glomerocrysts typically comprise monomineralic clots of clinopyroxene or plagioclase, or polymineralic clots of these two minerals, clinopyroxene having crystallised earliest. The glomerocrysts are taken as evidence for the dislodging of cumulate piles within one or more crustal staging chambers prior to or during eruption. No xenoliths, mafic enclaves, or glomerocrysts larger than a few mm were found.

Table 1. Summary of petrographic information from the Karkar monogenetic field. The sample details column records sample number, vesicularity (%), $^{40}Ar/^{39}Ar$ plateau ages for older Pleistocene lavas, plateau and inverse isochron ages for Late Pleistocene to Holocene lavas, and stages based on the most recent International Commission on Stratigraphy definition (Cohen et al. 2019). Mineralogy is presented in approximate order of occurrence, most common first.

Sample details	Co-ordinates	Overall texture	Groundmass	Phenocrysts
K16-1 ~5 % 332 ± 9 ka plateau Pleistocene-Middle	N39.744854 E45.939505	90-95% groundmass <0.25 mm 5-10% phenocrysts, rarely glomerocrysts 1-2 mm rare filled vesicles (calcite)	plagioclase, glass, oxides, apatite	clinopyroxene, plagioclase, amphibole (oxide rims), orthopyroxene
K16-2 ~2 % 152 ± 12 ka plateau Pleistocene-Late Middle	N39.736224 E45.950037	80% groundmass <0.3 mm 20% phenocrysts, some glomerocrysts 0.5-4 mm rare calcitised patches	plagioclase, clinopyroxene, oxides	plagioclase (sieve textured, concentric zoning), clinopyroxene, orthopyroxene (rimmed by clinopyroxene microlites)
K16-3 ~2-5 % 86 ± 10 ka plateau Pleistocene-Early Late	N39.753230 E46.017799	95% groundmass <0.3 mm 5% phenocrysts up to 5 mm hiatal texture	plagioclase, clinopyroxene, oxides, glass	plagioclase (sieve textured, faintly zoned), orthopyroxene
K16-4 ~10 % 9 ± 4 ka plateau Isochron 8 ± 3 ka Holocene-Greenlandian	N39.741133 E46.005302	80% groundmass <0.3 mm 20% phenocrysts, some glomerocrysts up to 4 mm	acicular plagioclase, oxides, glass	amphibole (oxide rims), plagioclase (sieve textured), rare clinopyroxene
K16-5 ~1-2 % 14 ± 4 ka plateau Isochron 16 ± 5 ka Pleistocene-Tarantian	N39.737838 E46.000792	85% groundmass ~0.3 mm 15% phenocrysts, some glomerocrysts up to 4 mm	acicular plagioclase, oxides, glass	amphibole (oxide rims), plagioclase (sieve textured), rare clinopyroxene
K16-6 ~1-2 % 13 ± 4 ka plateau Isochron 25 ± 9 ka Pleistocene-Tarantian	N39.721467 E46.006254	80% groundmass ~0.3 mm 20% phenocrysts, some glomerocrysts up to 4 mm	acicular plagioclase, oxides, glass, apatite	amphibole (oxide rims), plagioclase (sieve textured), rare clinopyroxene
K16-7 ~5-10 % 9 ± 3 ka plateau Isochron 6 ± 3 ka Greenlandian-Northgrippian	N39.717234 E46.008745	90% groundmass up to 1 mm 10% phenocrysts up to 3 mm	acicular plagioclase, oxides, amphibole, clinopyroxene, apatite	amphibole (oxide rims), plagioclase (sieve textured), rare clinopyroxene

4. Analytical methods

Samples for $^{40}Ar/^{39}Ar$ geochronology were initially prepared at the Scottish Universities Environmental Research Centre (SUERC) and Glasgow University. Each sample was pulverized by steel jaw crusher, sieved, rinsed in de-ionized water and dried. The 125 – 250 μm fraction was passed over by hand magnet before electrodynamic separation. Groundmass was carefully hand-picked under a binocular microscope to ensure, as far as possible, that phenocrysts including plagioclase and amphibole were not included in the final samples, each weighing several hundred mg. Samples and neutron flux monitors were packaged in copper foil and stacked in quartz tubes with the

relative positions of packets precisely measured for later reconstruction of neutron flux gradients. The sample package was irradiated in the Oregon State University reactor Cd-shielded facility. Alder Creek sanidine (1.1891 ± 0.0008 Ma (1σ), Niespolo et al. 2017) was used to monitor ^{39}Ar production and establish J values. At SUERC, gas was extracted from samples via step-heating using a mid-infrared (10.6 μm) CO_2 laser with a non-gaussian, uniform energy profile and a 3.5 mm beam diameter rastered over the sample well. The samples were housed in a doubly pumped ZnS-window laser cell and loaded into a copper planchette containing four 2.56 cm^2 wells. Liberated argon was purified of active gases, e.g., CO_2, H_2O, H_2, N_2, CH_4, using three Zr-Al getters; one at 16°C and two at 400°C. Data were collected on a Mass Analyser Products MAP-215-50 single-collector mass spectrometer using an electron multiplier collector in dynamic collection (peak hopping) mode. Time-intensity data were regressed to inlet time with second-order polynomial fits to the data. The average total system blank for laser extractions, measured between each sample run, was $4.8 \pm 0.1 \times 10^{-15}$ mol ^{40}Ar, $12.3 \pm 0.9 \times 10^{-17}$ mol ^{39}Ar, and $1.9 \pm 0.2 \times 10^{-17}$ mol ^{36}Ar. Mass discrimination was monitored daily, between and within sample runs, by analysis of an air standard aliquot delivered by an automated pipette. All blank, interference and mass discrimination corrections and age calculations were performed with the MassSpec software package (MassSpec, version 8.058, by Al Deino, Berkeley Geochronology Center). Decay constants are taken from Renne et al. (2011). Each sample was run in duplicate with each single analysis converted into a plateau age such that all included steps overlap in age within 2σ uncertainty, have a minimum n = 3, contain a minimum 50% of ^{39}Ar, and define an inverse isochron indistinguishable from the plateau age at 2σ uncertainty. Additionally, the trapped component composition, derived from the inverse isochron, is indistinguishable from air at 2σ. Age and uncertainty were defined by the mean weighted by the inverse variance of each step. The final plateau or isochron age was calculated using only the accepted plateau steps from the duplicate runs. A summary of results is presented in Table 2 and Figure 5, with full details available in Supplementary Items 1 (plateau and inverse isochron images) and 2 (raw and processed data).

Samples for whole rock geochemistry were crushed using a steel jaw crusher at the University of Glasgow and powdered to <100 μm using agate pots in a Retsch Planetary Ball Mill at the University of Cardiff. For major element chemistry, samples were analysed at the University of Edinburgh. Approximately 1 g of dried sample was ignited to 1100°C to calculate loss-on-ignition. A further unignited aliquot was heated with 5:1 borate flux in a platinum crucible to 1100°C for 20 minutes before cooling to room temperature. The original ratio was made up with fresh flux and the sample recast on a graphite plate. Discs were analysed on a Phillips PW2404 wavelength dispersive sequential x-ray spectrometer alongside a range of international standards for calibration and quality control. Analyses of international standard JB1a (n = 3; Govindaraju 1994) gave first relative standard deviations of <4 % for abundant major elements and <1 % for those present at ≤3 wt.%. Trace element solution geochemistry was conducted on an Agilent 7500ce mass spectrometer at the Scottish Universities Environmental Research Centre. Samples were dissolved using a $HF+HNO_3 + HClO_4 + HCl$ digestion procedure to ensure total dissolution of silicates and oxides. First relative standard deviations for all trace elements, were between 0.5 and 3 %, notwithstanding ~2 % estimated error in sample weighing and dilution, based on 25 replicate runs of international standard reference material BCR-2. Owing to limited time, a small amount of mineral-scale major element data was collected at the University of Manchester School of Earth and Environmental Sciences using a Cameca SX100 Electron Microprobe operating with 5 wavelength dispersive spectrometers at 15 kV. Calibration was carried out using a range of natural and synthetic minerals and oxides, with accuracy tested against secondary standards of augite, hornblende, plagioclase, jadeite and alkali feldspar. The microprobe study gathered two element maps covering around 0.5 cm^2 on K16-2 and K16-6, plus a few point and line scans from plagioclase crystals and more from phenocryst and groundmass clinopyroxene, intended for use in geobarometry.

5. Results

5.1. Geochronology

The seven samples all provided successful duplicate runs from which plateaux could be generated according to the criteria outlined in Section 4 (Table 2). The oldest sampled lava flow from the underlying volcanic units was dated to 332 ± 9 ka (plateau, K16-1), corresponding to the Middle Pleistocene. Flows immediately underlying the youngest activity have plateau ages of 152 ± 12 and 86 ± 10 ka (K16-2 and K16-3, respectively). The remaining four samples, K16-4 through 7, provided Latest Pleistocene to Holocene ages ranging from K16-5 (plateau 14 ± 4 ka, isochron 16 ± 5 ka) to K16-7 (plateau 9 ± 3 ka, isochron 6 ± 3 ka) (Figure 5). These youngest ages correspond with the stratigraphic relationships between flows as observed in the field. Eruptive centres are clearly visible on satellite imagery and follow an obvious NNW-SSE trend parallel to the strike of the local fault trends (Figure 2a). There is one discrepancy between the stratigraphic order of the older samples and the map developed by the

Institute for Geological Sciences. K16-2 is marked on Figure 2b as the first of the Holocene flows, but produced a late Middle Pleistocene plateau age. The location of K16-2 (Figure 2a) also appears to have more pronounced topographic expression and slightly better exposure compared to the subdued topography and poorer exposure of K16-3 (Figure 2a), implying that K16-3 should be the older of the two. However, K16-3 has a significantly younger plateau age dating it to the early Late Pleistocene, a discrepancy which does not appear related to the quality of the samples (Supplementary Item 1). One possible explanation for the greater extent of turf cover on the apparently younger dated sample (K16-3) is that the region of K16-3 has experienced downthrow since ~86 ka due to fault motion, leaving it prone to ponding of water and greater vegetative cover. The Holocene lavas may also have dammed Sev Lich, resulting in a wetter environment to the east of the younger lavas. The results from K16-7, Greenlandian to Northgrippian of the Holocene, also tally well with ages obtained from flows of the Karkar monogenetic field by cosmogenic ^{3}He dating, of 9.4 ± 2.4 ka and 5.2 ± 0.8 ka (2σ). These were reported by Avagyan et al. (2018) in a conference abstract, however the exact locations of these samples were not reported and cannot be directly compared with our study.

Table 2. Summary of Ar-Ar results for the Karkar monogenetic field. See text for analytical details, Figure 5 for representative plateaux and the Supplementary Item for full data.

Sample	Plateau age (ka) ± 2σ incl. J-value uncertainty	MSWD	Steps included	% total gas	Mol ^{39}Ar	Plateau Ca/K ± 2σ	Isochron age (ka) ± 2σ incl. J-value uncertainty	MSWD	p	^{40}Ar/^{36}Ar$_{(i)}$ ± 2σ
K16-1 aliquot 1	334 ± 10	1.2	25/33	88.1	6.2E-13	1.01 ± 0.01	363 ± 24	0.9	0.53	296.5 ± 1.6
K16-1 aliquot 2	324 ± 19	1.1	18/30	71.0	2.3E-13	0.97 ± 0.02	323 ± 52	1.1	0.32	298.6 ± 2.2
K16-1 composite	**332 ± 9**	**1.1**	**43/63**		8.6E-13	**1.01 ± 0.01**	**353 ± 20**	**1.0**	**0.41**	**297.2 ± 1.2**
K16-2 aliquot 1	139 ± 36	0.8	13/17	98.0	5.8E-14	2.29 ± 0.08	202 ± 118	0.9	0.59	295.6 ± 14.3
K16-2 aliquot 2	154 ± 13	0.9	36/38	93.0	7.3E-13	2.53 ± 0.03	185 ± 40	0.9	0.69	297.4 ± 1.9
K16-2 composite	**152 ± 12**	**0.9**	**49/55**		7.9E-13	**2.51 ± 0.03**	**177 ± 36**	**0.9**	**0.76**	**297.6 ± 1.8**
K16-3 aliquot 1	70 ± 30	1.0	17/17	100.0	7.0E-14	21.3 ± 2.1	127 ± 58	1.0	0.47	295.2 ± 7.1
K16-3 aliquot 2	88 ± 10	1.1	25/42	75.1	6.7E-13	0.99 ± 0.01	135 ± 40	1.0	0.43	295.8 ± 3.4
K16-3 composite	**86 ± 10**	**1.1**	**42/59**		7.4E-13	**7.67 ± 0.26**	**135 ± 33**	**1.0**	**0.49**	**295.7 ± 3.0**
K16-4 aliquot 1	17 ± 16	1.2	12/17	96.4	6.4E-14	1.02 ± 0.04	4 ± 3	1.2	0.27	302.9 ± 14.5
K16-4 aliquot 2	9 ± 4	1.2	23/33	90.1	8.6E-13	0.95 ± 0.01	8 ± 4	1.2	0.21	298.6 ± 4.2
K16-4 composite	**9 ± 4**	**1.2**	**35/50**		9.2E-13	**0.96 ± 0.01**	**8 ± 3**	**1.2**	**0.20**	**299.0 ± 4.5**
K16-5 aliquot 1	13 ± 5	1.1	17/17	100.0	8.9E-13	1.70 ± 0.01	17 ± 8	1.1	0.32	297.5 ± 3.2
K16-5 aliquot 2	15 ± 8	1.0	11/20	95.6	7.9E-13	1.37 ± 0.01	24 ± 13	1.0	0.44	297.3 ± 2.9
K16-5 composite	**14 ± 4**	**1.0**	**28/37**		1.7E-12	**1.58 ± 0.01**	**16 ± 5**	**1.0**	**0.42**	**298.0 ± 1.8**
K16-6 aliquot 1	16 ± 6	0.7	12/17	94.7	8.1E-13	1.49 ± 0.01	32 ± 19	0.6	0.83	295.0 ± 6.1
K16-6 aliquot 2	9 ± 7	0.6	14/20	97.5	8.5E-13	1.26 ± 0.01	19 ± 12	0.6	0.88	297.1 ± 2.9
K16-6 composite	**13 ± 4**	**0.7**	**26/37**		1.7E-12	**1.39 ± 0.01**	**25 ± 9**	**0.6**	**0.96**	**296.3 ± 2.3**
K16-7 aliquot 1	11 ± 5	0.8	13/17	85.4	7.6E-13	1.22 ± 0.01	2 ± 1	0.7	0.75	301.8 ± 5.1
K16-7 aliquot 2	6 ± 5	1.0	7/21	71.6	6.8E-13	0.82 ± 0.01	12 ± 10	1.2	0.31	296.6 ± 7.6
K16-7 composite	**9 ± 3**	**0.9**	**20/38**		1.4E-12	**1.10 ± 0.01**	**6 ± 3**	**1.0**	**0.50**	**299.6 ± 4.1**

Figure 5. Representative Ar age plateau and isochron diagrams for the two apparently youngest samples, K16-4 and K16-7. Full data are presented in the Supplementary Item.

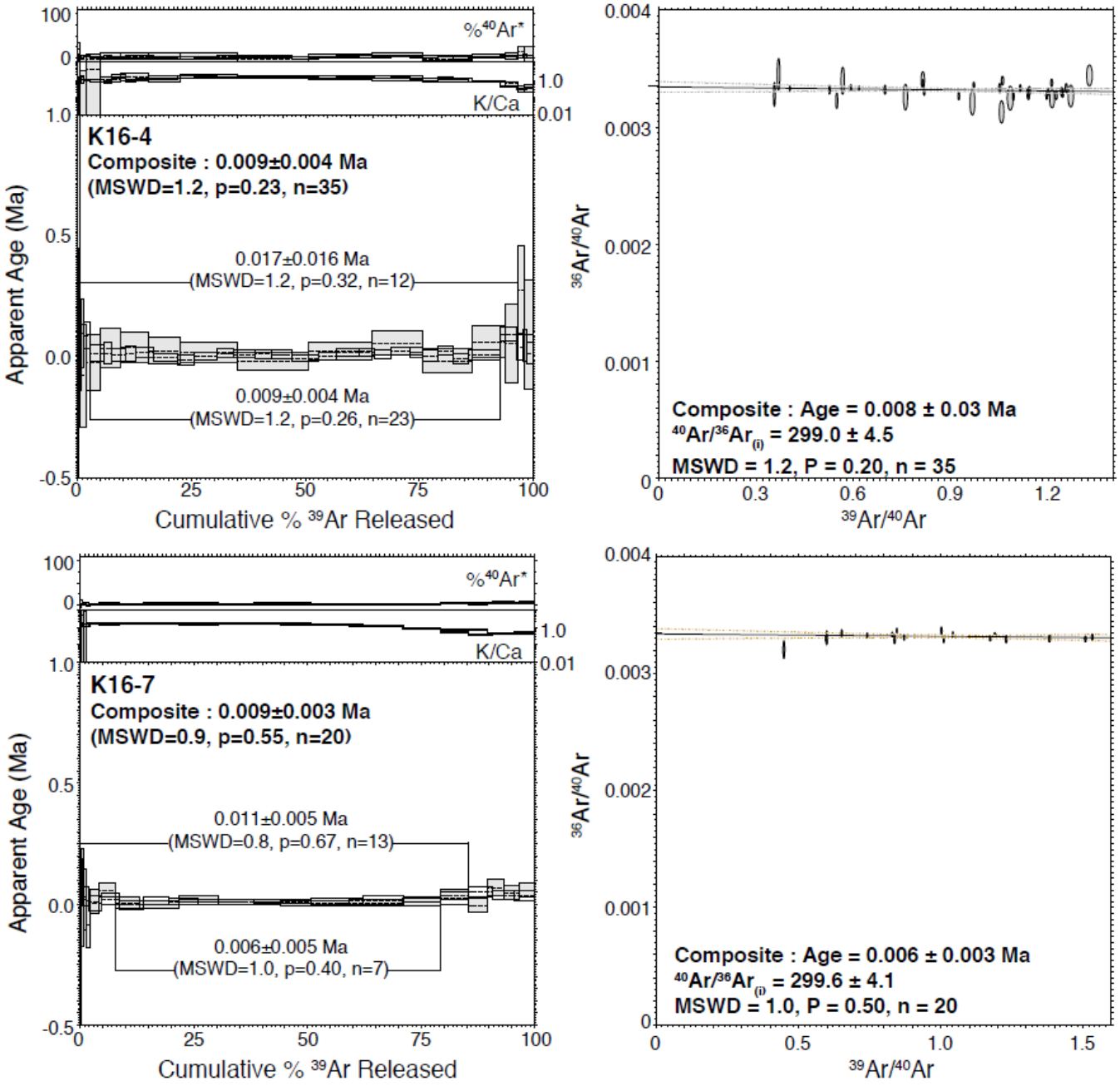

5.2. Whole rock geochemistry

The Karkar Group samples are alkaline (Figure 6a) and shoshonitic (Figure 6b) with K_2O of ~3 wt.% and SiO_2 ranging from 53 to 58 wt.% (Table 3). Samples display subtle major- and trace-element differences between the four latest Pleistocene-Holocene (K16-4 through 7) and the three older Pleistocene samples (K16-1 through 3). The oldest samples have evolved trachyandesitic compositions, whereas the youngest samples plot uniformly as less evolved trachybasaltic andesites. All have MgO < 4 wt.%, but the trachyandesites have lower Al_2O_3, Fe_2O_3, MgO, Na_2O, TiO_2 and P_2O_5 concentrations and slightly higher CaO compared with the younger trachybasaltic andesites (Table 3). All samples and fall in the 'Syunik' field of collision-related Quaternary volcanism of Sugden et al. (2019), who analysed Pleistocene lavas, scoria and ignimbrites from both mono- and polygenetic centres across Syunik, but not Karkar. The Karkar and Sugden et al. (2019) suites are conspicuous for their high abundance of P_2O_5 compared to Pleistocene samples from elsewhere in Armenia (0.6-1.0 wt.%).

Table 3. Major and trace element geochemistry of samples from the Karkar monogenetic field. Major element oxides are reported in wt.%, trace elements in parts per million. LOI – loss on ignition. (t) – total iron.

Sample	K16-1	K16-2	K16-3	K16-4	K16-5	K16-6	K16-7

SiO_2	55.48	55.22	58.49	53.33	53.76	54.76	53.20
TiO_2	0.882	0.818	0.855	1.089	1.106	1.062	1.121
Al_2O_3	16.10	15.44	16.11	16.50	16.71	16.68	16.45
Fe_2O_3 (t)	7.56	7.13	7.28	8.67	8.28	7.80	8.36
MnO	0.122	0.113	0.113	0.127	0.127	0.122	0.128
MgO	3.47	3.25	3.18	3.64	3.67	3.52	3.88
CaO	7.56	7.49	5.34	6.95	6.77	6.64	6.99
NaO	4.32	4.01	4.31	4.45	4.45	4.45	4.53
K_2O	3.219	2.823	3.150	2.981	3.038	3.089	3.128
P_2O_5	0.836	0.585	0.566	0.949	0.945	0.921	1.024
LOI	0.00	2.64	0.00	0.95	0.63	0.57	0.78
Total	99.51	99.39	99.64	99.49	99.62	99.59	99.59
Sc	10.2	10.1	9.9	11.4	11.7	13.1	10.6
V	39.6	35.0	44.0	32.2	34.6	33.7	47.9
Cr	39.6	50.3	115.6	40.2	49.0	47.1	87.6
Co	25.2	23.6	24.5	29.1	28.9	28.1	29.9
Ni	61.8	104.5	134.3	121.1	191.8	161.6	212.3
Rb	51.4	45.9	52.1	40.4	38.9	38.9	36.1
Sr	679	967	1110	1184	1883	1616	2381
Y	18.4	15.8	18.0	20.0	21.0	20.8	20.4
Zr	182.8	156.0	180.3	196.2	207.5	206.1	205.2
Nb	23.9	18.8	19.6	24.8	26.1	25.7	27.4
Ba	1038	853	844	1064	1073	1103	1166
Hf	4.0	3.5	4.0	4.3	4.5	4.6	4.5
Ta	0.8	0.7	0.7	0.8	0.8	0.8	0.9
Pb	13.0	12.1	13.1	12.9	13.0	13.5	13.7
Th	9.5	9.2	9.5	6.9	6.9	7.1	6.9
U	2.2	2.3	2.2	1.6	1.6	1.6	1.6
La	76.4	58.6	59.4	80.1	81.8	81.9	86.1
Ce	141.2	107.0	105.5	152.2	153.8	154.1	163.8
Pr	15.0	11.1	11.0	16.3	16.7	16.6	18.2
Nd	52.0	38.4	38.1	57.2	58.1	58.0	64.0
Sm	7.6	5.9	5.9	8.4	8.6	8.5	9.2
Eu	2.0	1.6	1.7	2.2	2.3	2.3	2.5
Gd	6.7	5.3	5.5	7.3	7.5	7.4	8.0
Tb	0.7	0.6	0.7	0.8	0.8	0.8	0.9
Dy	3.5	3.2	3.4	3.7	3.8	3.7	3.9
Ho	0.6	0.6	0.6	0.7	0.7	0.7	0.7
Er	1.8	1.7	1.8	1.8	1.8	1.8	1.8
Tm	0.3	0.3	0.3	0.3	0.3	0.3	0.3
Yb	1.6	1.6	1.7	1.6	1.6	1.6	1.6
Lu	0.3	0.2	0.3	0.2	0.2	0.2	0.2

Chondrite-normalised plots (Figure 6c) demonstrate that the older, evolved samples have lower abundances of all REE (rare earth elements) except for the HREE (heavy REE) Yb and Lu. Both suites have quite flat HREE patterns and very steep, LREE (light REE)-enriched characteristics, with La/Yb_{CN} ranging from 24-37, the older samples having the lowest ratios. There are small negative Eu anomalies in each sample, with Eu/Eu^*_{CN} ranging from 0.86-0.89. On a primitive mantle-normalised plot (Figure 6d), samples again mirror others from across Syunik in having negative Nb-Ta anomalies and 'spiky' patterns typical of subduction-related settings (Sugden et al. 2019). The older, evolved samples have higher Th and K concentrations, but lower Ba, Sr, and HFSE (high field strength elements, incl. Nb, Ta, Zr and Hf) compared to the younger, less evolved samples. The conspicuous positive Zr-Hf anomaly that has been noted elsewhere in Armenia (Neill et al. 2013) was not picked out here, possibly due to the very incompatible element-enriched nature of the samples. Absolute Zr ranges from 180-207 ppm, with high Zr/Hf ratios of 44-46, matching most other samples with similar SiO_2 across Armenia (Sugden et al. 2019).

Figure 6. a) Total alkali-silica plot after Le Bas et al. (1986) showing Syunik (southern Armenia) and Shirak/Lori (northern Armenia) fields after Sugden et al. (2019). b) K_2O vs. silica classification plot after Peccerillo and Taylor

(1976). c) Chondrite-normalised plot using normalisation of McDonough and Sun (1995). d) Primitive Mantle-normalised plot using normalisation of Sun and McDonough (1989).

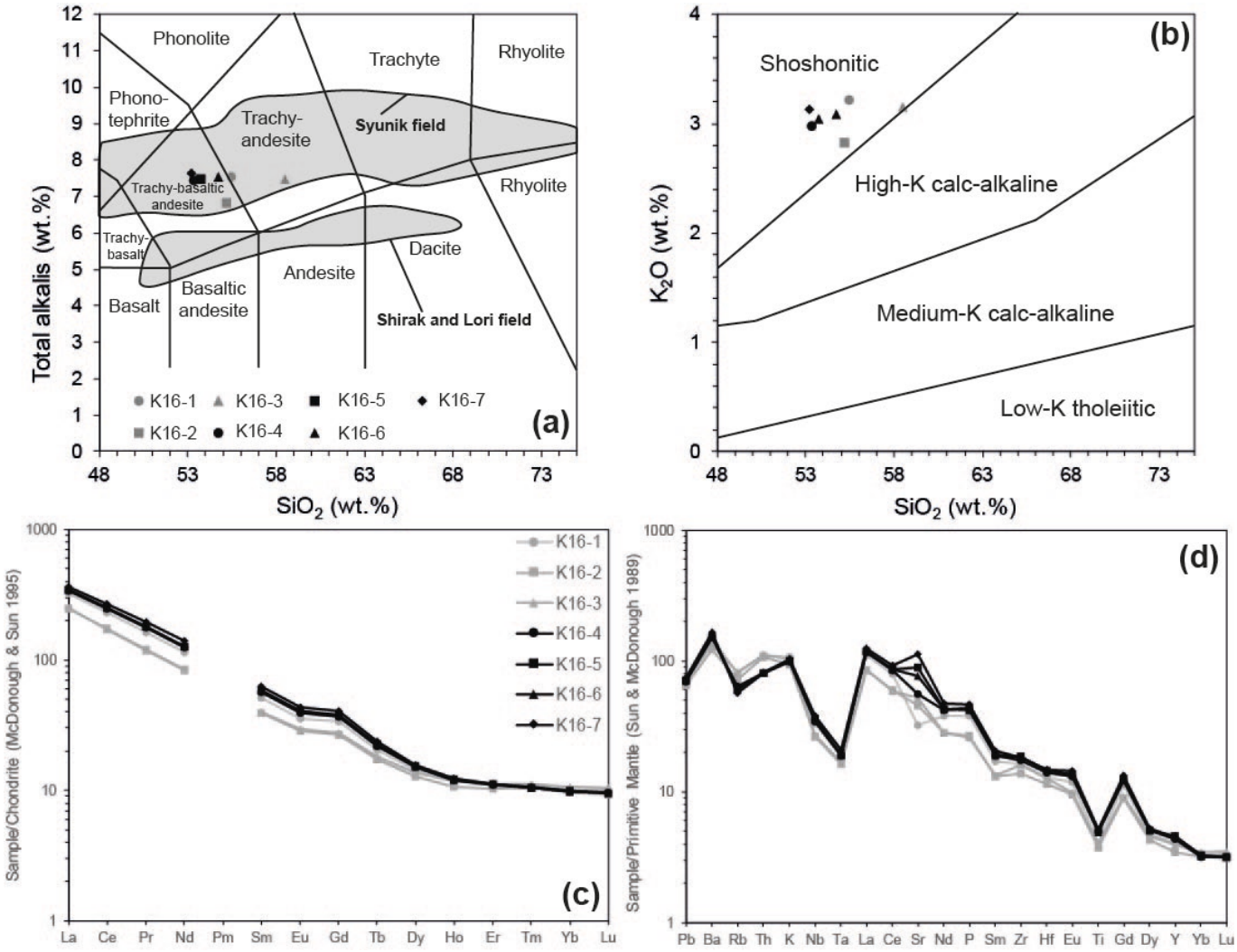

5.3. Mineral chemistry

The two element maps from K16-2 (Pleistocene) and K16-6 (Holocene) are shown in Figure 7 along with extracted plagioclase anorthite proportions and pyroxene CaO wt.% concentrations from several transects. Additionally, plagioclase anorthite contents in a single line scan of K16-2 oscillated between An_{40}-An_{46}, and a range of plagioclases included close to the margins of analysed clinopyroxene crystals also typically ranged from An_{35}-An_{57}. The element map for K16-2 shows extensive zoning and sieve texturing in the large plagioclase crystals, as well as the growth of a very thin and sharp outer rim beyond the sieve texturing which is of higher anorthite content than the rest of the crystals. Unfortunately, the textural disruption of these zones' crystals prevented diffusion modelling work, and no orthopyroxenes (e.g. Chamberlain et al. 2014) were analysed. The mapped clinopyroxene glomerocryst in K16-6 shows little visual compositional variation or layering, but multiple transects reveal oscillatory zoning with no overall pattern from core to rim. The patterns shown in K16-2 are consistent with recharge and fractional crystallisation in a magma reservoir followed by equilibration with a higher CaO melt, probably during mixing and final ascent, but it is clear that not all crystals have picked up these patterns and that some are likely to be antecrystic in origin.

Figure 7. Element maps showing (top) K16-2 (Pleistocene) and (bottom) K16-6 (Holocene). K16-2 shows oscillatory zoning in two large plagioclase crystals, with evident sieve texturing and heterogeneous anorthite concentrations. Line 1 (with inclusions removed) demonstrates late growth of high-Ca plagioclase perhaps indicative of magma mixing, whilst Line 2 may represent an antecryst which shows little internal zonation and much lower anorthite contents. K16-6 is a typical clinopyroxene glomerocryst displaying only subtle oscillatory zoning.

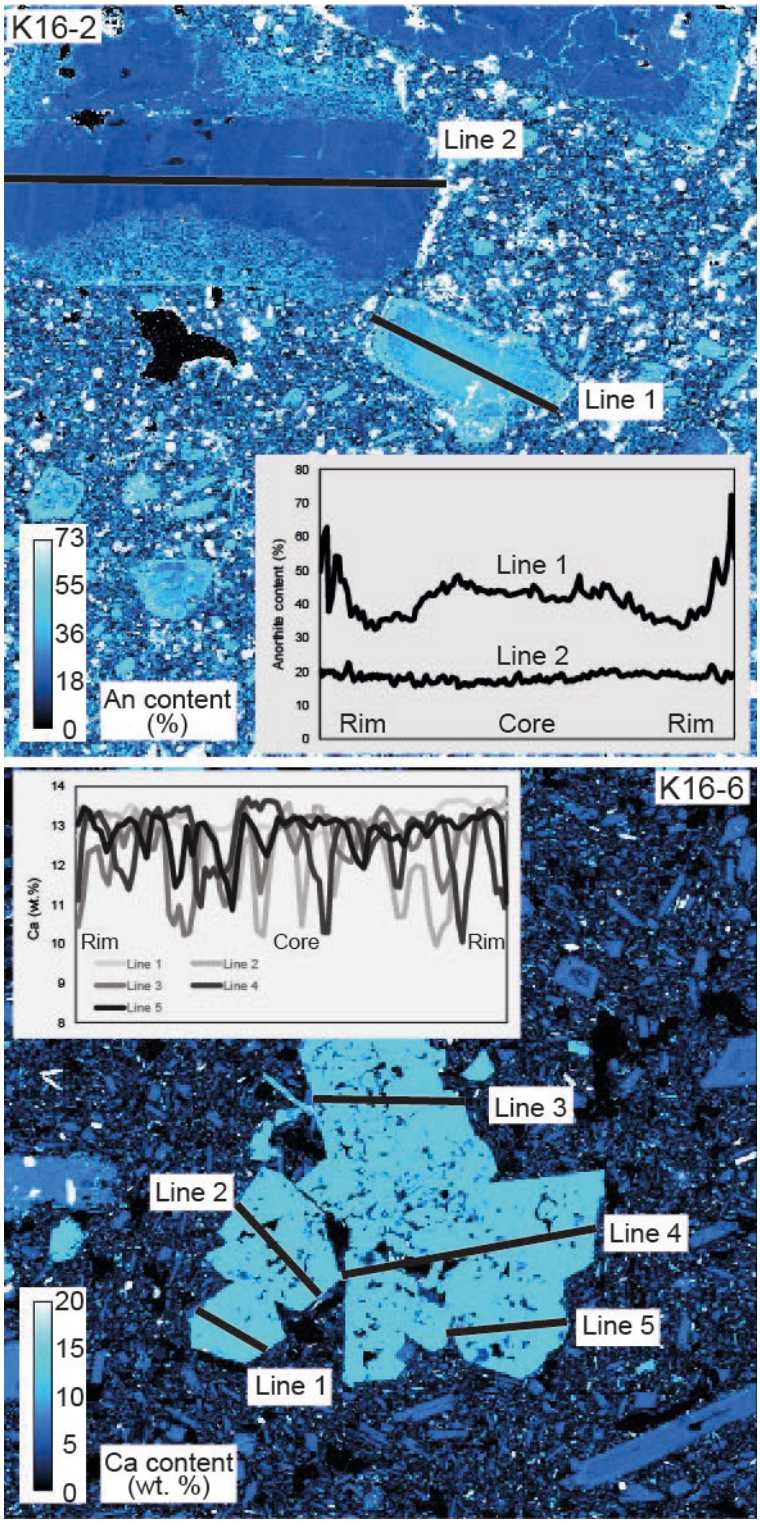

Microprobe time was also briefly used to gather compositional data from the cores of clinopyroxene phenocrysts and some larger groundmass grains. We applied the CpxBar Excel spreadsheet of Nimis (2000), based on Nimis (1999), to calculate approximate pressures of crystallisation in K16-2 (Pleistocene) and K16-5 and 6 (Latest Pleistocene-Holocene). The specific calibration used in CpxBar was one intended for moderately alkaline magmas, although it is highly sensitive in inverse proportion to temperature and requires T as an independent input. In the absence of our own thermometry data we followed Sugden et al. (2019), who proposed that the southern Lesser Caucasus magmas were generated at ~1200°C in the mantle lithosphere. Using the slope of the mantle adiabat, we assume magmas would be erupted at ~1150°C without additional cooling in the crust. Using 1150°C as the input value for T provided a cluster of pressures of between 1.5-2.5 ± 2 kbar, very roughly equating to 5-9 km depth, with a fairly continuous range of pressures from 3-7 ± 2 kbar, i.e. roughly between 7-26 km. The oldest sample, K16-2, consistently provided the highest pressures of the three samples, which implies perhaps deeper storage of

the earlier magmas. This very preliminary finding is at least consistent with mid-crustal amphibole fractionation and the resulting paucity of amphibole in the oldest samples. Again, a tentative conclusion is that many clinopyroxenes crystallised at comparatively low pressure in the upper crust, and we posit that a shallow (less than 10 km) magma reservoir could be identified with passive seismic monitoring. If detected, this may help resolve the dispute over the heat source for the geothermal system (c.f. White et al. 2015; Gilliland et al. 2018).

6. Discussion

6.1. A Holocene eruption record at Karkar

Archaeological evidence presented in Karakhanian et al. (2002) has previously been used to justify very young magmatism at Karkar. In brief, lava blocks of the youngest flow generation were said to have covered loam associated with obsidian tools, bones and ceramic materials, from which a ^{14}C age of 4720 ± 140 yr was revealed (the nature of the reported error was not mentioned). The new inverse isochron $^{40}Ar/^{39}Ar$ date for K16-7 of 6 ± 3 ka lies within error of this archaeological age. However, the archaeological age is not within error of the plateau age from the same sample, of 9 ± 3 ka. Although we cannot rule out the possibility that the loam sample was contaminated by younger sources of carbon, we can also suggest that the plateau age may record a slightly radiogenic trapped Ar component. In that situation we would consider the inverse isochron age more acceptable. At the very least, the inverse isochron $^{40}Ar/^{39}Ar$ dates for both K16-4 and K16-7 are, respectively, well within 2σ error of the aforementioned cosmogenic ^{3}He ages of 9.4 ± 2.4 ka and 5.2 ± 0.8 ka (Avagyan et al. 2018). We caution that the true uncertainty of these ^{3}He ages may be higher than reported, given uncertainties in production scaling and shielding effects, but overall, we have strong confidence that at least two Holocene eruptions took place at Karkar. All the reported evidence, be it archaeological, radiometric, or cosmogenic, may require further verification to pin down the precise age of the last eruptions at Karkar.

With a few km of Karkar and at many sites across Armenia are exceptional petroglyphs made in the sleek patina of volcanic blocks (Knoll et al. 2013). The carvings, including animals, hunting scenes and human figures, have proven difficult to date beyond qualitative comparison with occurrences elsewhere in the region (Knoll et al. 2013 and discussion in Karakhanian et al. 1997). Between Karkar and Porak volcano 40 km to the north-west, Karakhanian et al. (2002) describe a petroglyph then tentatively ascribed to the 5th millennium BC. The features have been interpreted as a depiction of strombolian-style fire fountaining at a nearby volcano, usually attributed to eruption of Porak (Karakhanian et al., 2002), and represent amongst some of the world's oldest representations of a volcanic eruption. However, Avagyan et al. (2018) also report a ^{3}He age of 28 ± 12 ka (2σ) for their argued youngest eruption of the main cone of Porak, in direct contrast to the 3.7 ± 4.2 ka (2σ) $^{40}Ar/^{39}Ar$ age reported in the same abstract volume for a fissure eruption ~8 km north of the cone by Meliksetian et al. (2018). Therefore, although it is not clear which eruption is being depicted by the petroglyphs, it is nevertheless almost certain that inhabitants of the uplands between Lake Sevan and Karkar experienced volcanic activity first-hand. Fountaining behaviour and development of scoria cones would have been visible for many km around and were probably accompanied by moderate earthquakes associated with opening of volcanic fissures. In the example the Great Tolbachik fissure eruption of 1975, these reached magnitudes of ~5.5 (Fedotov et al. 1976; Zobin and Gorelchik 1982). It is unclear if these events would provide any immediate threat to life, but events may have been locally disruptive and would have formed an intrinsic part of local heritage (Karakhanian et al. 2002).

We think it now critical that precise and accurate ages are obtained and published for the very youngest ranges of activity at Karkar, Porak, Smbatassar and the seismically-active Gegham Ridge in order to complete the Holocene volcanic record in central to south Armenia and allow for better calculation of the probability for lava flow inundation. This is no small undertaking. The $^{40}Ar/^{39}Ar$ method has proven effective here, but there is a lack of groundmass sanidine which is widely considered the optimum material for analysis. Furthermore, although we took considerable care to avoid any lavas with secondary mineralisation, it is possible that improved results could be obtained by cutting into the dense interior of flows. Further care in sample selection and processing, and perhaps running samples in triplicate, may provide further marginal improvements in precision. Given uncertainties in winter snow cover during the past 10 ka, we caution that cosmogenic isotope ages may be subject to more significant uncertainty (Delunel et al. 2014). Although some archaeological ^{14}C ages from soil layers have previously been published, these are difficult to obtain from beneath thick lava flows owing to very low vegetation levels, and the possibility of contamination from recent carbon sources should be considered as a factor in discrepancy between the $^{40}Ar/^{39}Ar$ and cosmogenic ages for Nazeli and the ^{14}C age reported in Karakhanian et al. (2002).

It is pertinent to query whether this 'active' volcanism presents material hazards to the local region. The edifices and fissures are spatially entirely restricted to fault zones undergoing active extension (Karakhanian et al. 1997) and the most common eruptive mode is for one or two effusive to weakly pyroclastic events to occur in a volcanic cycle. Lava volumes appear to be small (in the order of <<0.1 km^3 per flow) and most flows only travel a few km. Lava inundation should be nevertheless be considered in natural hazard assessments and preparations. Relevant sites would include the immediate vicinity of any new or existing geothermal infrastructure at Karkar or future infrastructure at Porak, the main Armenia-Iran highway south of Yeghednadzor near to Vayots Sar and Smbatassar, and Vardenis town and surrounding villages and roads on the northern flank of Porak. We will discuss Porak, Vayots Sar and Smbatassar in more detail in future communications.

6.2. Petrogenesis of the Karkar magmas

The current hypothesis for magma genesis beneath the South Caucasus involves sources within the mantle lithosphere. Sugden et al. (2019) argued that in the south of Armenia, where the lithospheric thickness is >100 km, melting has taken place due to a dehydration reaction as thickened, subduction-modified lithosphere crosses the amphibole peridotite solidus. This is an application of a model that may be more widely applicable for the generation of mafic melts in active collision zones (Allen et al. 2013). Predictably given the short eruption timescale, the youngest samples do not define meaningful evolutionary trends on the total alkali-silica diagram (Fig. 6a) and even the older samples cluster together despite having an age range of ~250 ka. The youngest samples are the most mafic (~53 wt.% SiO_2), but only contain 3-4 wt.% MgO so if derived from an ultramafic parent will have fractionated at least olivine, clinopyroxene ± amphibole ± plagioclase and would require very imprecise back-projection for petrogenetic calculations. As such, we have not attempted to model the source and partial melting conditions of the Karkar lavas further. Suffice to note, their typical 'spiky', light REE-enriched normalised patterns with negative Nb-Ta anomalies (Fig. 6d) are entirely consistent with the proposed source of magmas across Armenia (Sugden et al. 2019). Comparatively steep heavy REE patterns (Fig. 6c) concur with the Sugden et al. (2019) hypothesis that magmatism in Syunik is derived from depths within the garnet-spinel transition zone.

Considering the relationship between the Late Pleistocene-Holocene flows and the older Pleistocene flows: are the two suites part of the same magma plumbing system connected by fractional crystallisation (FC) and assimilation processes over a few 100s of ka? The younger samples are slightly less evolved than the oldest lavas (53-55 wt.% vs. 55-58 wt.% SiO_2) and there are differences in both mineralogy and trace element chemistry. The younger lavas have abundant amphibole phenocrysts, and contain higher concentrations of Al and most trace elements, particularly Ba and Sr, with the exception of having lower Ca, Rb and Th. When compared on Figure 8, the youngest samples fall clearly within the Syunik field of Sugden et al. (2019) but the older samples lie slightly above it in the geographically and chemically defined 'Vardenis' field which includes eruptions near the modern Porak volcano. Figure 8 compares all analysed volcanic samples of mafic to felsic composition and demonstrates reasonably good trends for each field which may be explained by FC processes. However, at Karkar, the older and younger samples do not lie on a typical FC trend.

Amphibole and plagioclase fractionation or accumulation may be partly responsible for such variations; in particular the Dy/Yb (~1.5-1.6 vs. 1.3-1.4) and Dy/Dy* ratios (~0.52 vs. 0.49) of the younger, amphibole-rich samples are higher than those of the older, amphibole-free samples (Davidson et al. 2013). A greater proportion of plagioclase fractionation affecting the older lavas could explain their lower Al and Sr concentrations, but both suites have similar geometric Eu anomalies (Eu/Eu* = 0.86-0.89) which may be explained by amphibole fractionation lowering middle REE concentrations in the older samples and thus hiding the relative Eu/Eu* anomaly. However, such changes cannot be responsible for other differences between the suites: the higher proportions of light REE, P, Zr-Hf and lower Rb and Th in the younger samples are not easily explained as none are compatible in amphibole, clinopyroxene or plagioclase. The older samples may have also experienced crustal contamination, especially if they were evolving in the middle crust for a greater time than the younger ones, consistent with the general lack of amphibole. Rb and Th are especially abundant in the middle to upper crust and are noticeably higher in the older samples (e.g. 46-52 ppm Rb vs. 36-40 ppm). The noticeably lower Nb-Ta and Zr-Hf in the older more evolved samples may also relate to crustal contamination being a greater factor in the petrogenesis of the older samples, given the middle crust does tend to have lower high field strength element (HFSE) abundances compared to these magmas (Rudnick and Fountain, 1995; Taylor and McLennan, 1985). It should be pointed out that crustal contamination is a moderately rare feature of Quaternary Armenian magmatism as determined by isotopic studies (Neill et al., 2015; Sugden et al. 2019) and therefore an alternative explanation

may be possible. We suggest that the mantle source(s) of magmatism become progressively depleted and dehydrated over the last ~0.3 Myr, and therefore less concentrated in subduction-mobile elements such as Rb and Th. The effect of this progression would be to lower Th/Yb ratios and Rb in the youngest samples. As the mantle progressively dehydrates, a smaller degree of partial melting would also be expected, resulting in the higher LREE, P and HFSE abundances of the youngest lavas. We suspect that a combination of these discussed factors may be responsible for the difference between the two suites of lavas, and that a longer time-span of magmatic activity at single sites should be analysed in greater detail, including with radiogenic isotope analyses, to determine if there are genuine systematic changes in partial melting conditions and storage depths and timescales beneath Armenia.

Figure 8. Th/Yb vs. Ta/Yb after Pearce (1983) with fields and vectors from Sugden et al. (2019). The youngest Karkar lavas fall clearly within the Syunik field, whereas the older lavas lie just above this field, similar to Vardenis, the location of the Holocene Porak volcano. The FC vector was generated by Sugden et al. (2019) based on fractionation of clinopyroxene, amphibole and plagioclase using modified partition coefficients to account for the change from mafic to more evolved compositions.

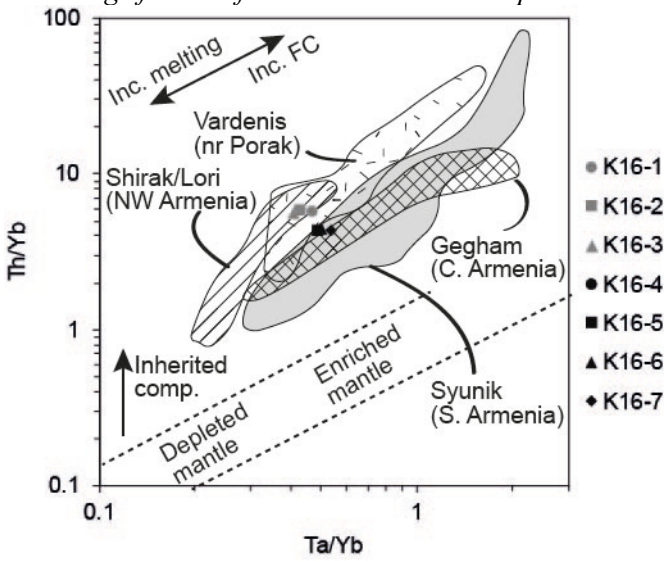

6.3. Geothermal energy potential and future study

The two boreholes have encountered temperatures sufficient for geothermal power generation, but insufficient porosity in the host rocks at such depths. The wells have been recommended for deeper drilling if electricity generation is to be a reality (Gilliland et al. 2018). More thorough petrological, geochronological and geophysical techniques may be applied to understand more fully the Karkar system. Recent eruptions are directly related to actively extending components of the PSSF system, but the magmas which ascended these faults have previously been stored in the crust, perhaps at quite shallow depths of << 10 km. It would be appropriate to do more detailed geobarometry and geothermometry to properly constrain storage depths, and to engage passive seismic monitoring as a means of determining the precise location of current magma reservoirs. We do not know the age or emplacement history of the Dalidagh body or the quartz monzonite, so they are critical targets in establishing whether these intrusive rocks are truly the heat source, or if it is a separate magma chamber or chambers associated with the youngest Holocene volcanism. Collectively such studies should enable better targeting of future drilling to identify sustainable heat sources. We also think a more thorough petrographic review is necessary to establish if magma mixing is a viable eruption trigger, over what timescales this occurs (geospeedometry) and whether magma mixing might therefore be detectable, using geophysical methods, as a precursor to future eruptions. A further geological consideration relevant to Karkar is the extent to which ice unloading may be a factor in assisting volcanism given that at least two eruptions took place at the end of the Pleistocene and beginning of the Holocene. Ollivier et al. (2010) have already documented numerous moraines associated with retreat following the last glaciation, at ~1500 m and above, and the uplands across much of the South Caucasus were at one time extensively glaciated (Messager et al. 2013). Therefore, we posit that much more detailed geochronology will establish if eruptive activity spiked during this period and has since waned, or if the eruption rate has remained consistent and likely tectonically controlled, independent of glacial activity.

Finally, given the promising young $^{40}Ar/^{39}Ar$ age result for Porak volcano north of Karkar on the PSSF which lies firmly within the Holocene, we consider this very similar volcanic centre equally, if not more promising for

geothermal energy exploration and development (Meliksetian et al. 2018). As stated by Gilliland et al. (2018), Karkar may be a future site for electricity generation with deeper drilling, but we note it is distant from nearby larger towns which might benefit from district heating schemes. The nearest villages are over 15 km away (e.g. Sarnakunk), each with fewer than 500 inhabitants, necessitating further development for more transportable electricity supplies. In contrast, at Porak, a new geothermal development on the heathlands immediately north of Porak summit would be within 10 km of Vardenis, with a population of over 12,000, and various small villages each with populations of over 1000 may benefit both from district heating and electricity generation.

7. Conclusions

The Karkar monogenetic field in Syunik, SE Armenia consists of Pleistocene to Holocene lava flows erupted through fault-controlled volcanic conduits and exhibiting weak fountaining behaviour. These were erupted on top of a succession of poorly dated intrusive rocks and ophiolitic materials. The Pleistocene-Holocene activity is associated with a pull-apart structure on the right-lateral Syunik branch of the trans-national Pambak-Sevan-Syunik Fault. Ultimately, the magmas were derived by small volume melting of the lithospheric mantle beneath this region, and extensive fractionation during magma ascent, particularly in the middle to upper crust. The Karkar monogenetic field is Armenia's first test drilling site to judge the feasibility of high-temperature geothermal energy production. We add to previous published and unpublished views in corroborating a Holocene age for the youngest eruptions. Karkar and neighbouring volcanic fields should be considered with high certainty as an active volcanic region and therefore more thorough dating, geophysical monitoring and risk assessments for current and future infrastructure should be considered, which would also factor into constraining the most appropriate sustainable locations for future drilling. Finally, we can only speculate at this time as to the relative role of tectonism and ice unloading in the timing and extent of magmatic activity, and we suggest additional dating will help resolve this question.

Acknowledgements

This paper is dedicated to our much-respected colleague and collaborator Arkady Karakhanian who died suddenly in Yerevan in 2017. The Armenian team and IN were supported by the Armenian State Committee for Science. IN was supported by the Carnegie Trust for the Universities of Scotland [Research Incentive Grant 70419, 2016] and the Geological Society of London [Elspeth Matthews Fund, 2016]. EM received an Angus Mitchell Scholarship for MSc research and the Sir Alwyn Williams fund for postgraduate research, both at the University of Glasgow. Bob Gooday conducted sample powdering at Cardiff University. Sponsors had no role in project design, implementation or publishing decisions.

References

Avagyan A., Ritz J.-F., Blard P.-H., Meliksetian Kh., Munch P., Valla P., Tokhatyan K.S., Mkrtchyan M., Atalyan T. 2018. Volcanic eruptions witnessed by prehistoric people in Armenia. Conference Abstract Volume; Ancient Armenia at the Crossroads, 6-7 Nov. 2018, Lyon, France, p. 15-16.

Balasanyan, S., Karakhanyan, A., Meliksetian, Kh. 2018. Archaeoseismological studies of the eastern branch of the Syunik pull-apart basin structure. Conference Abstract Volume; Ancient Armenia at the Crossroads, 6-7 Nov. 2018, Lyon, France, p.17.

Chamberlain, K.J., Morgan, D.J., Wilson, C.J.N. 2014. Timescales of mixing and mobilization in the Bishop Tuff magma body: perspectives from diffusion chronometry. Contributions to Mineralogy and Petrology 168, 1034.

Cohen, K.M., Finney, S.C., Gibbard, P.L., Fan, J.-X. (2019; updated). The ICS International Chronostratigraphic Chart. Episodes 36, 199-204, available at https://stratigraphy.org/index.php/ics-chart-timescale.

Davidson, J.P., Turner, S., Plank, T. 2013. Dy/Dy*: Variations arising from mantle sources and petrogenetic processes. Journal of Petrology 54, 525-537.

Delunel, R., Bourles, D.L., van der Beek, P.A., Schlunegger, F., Leya, I., Masarik, J., Paquet, E. 2014. Snow shielding factors for cosmogenic nuclide dating inferred from long-term neutron detector monitoring. Quaternary Geochronology 24, 16-26.

Fedotov S., Khrenov, A., Chirkov, A., 1976. The Great Tolbachik Fissure Eruption, Kamchatka, 1975. Doklady Akademii Nauk SSSR V. 228, 5. p. 1193-1196.

Galoyan, G. Rolland, Y., Sosson, M., Corsini, M., Melkonyan, R. 2007. Evidence for superposed MORB, oceanic plateau and volcanic arc series in the Lesser Caucasus (Stepanavan, Armenia). Comptes Rendus Geoscience 339, 482-492.

GeoRisk, 2012. Independent interpretation of the results of the 3D MT, gravity and CO_2 surveys conducted at the Karkar Site. Armenia Geothermal Project Report GEF-CS4-2008 to the Armenian Government, Yerevan, 170 pp.

Gevorgyan, H., Repstock, A., Schulz, B., Meliksetian, Kh., Breitkruez, C., Israyelyan, A. 2018. Decoding a postcollisional multi-stage magma system: The Quaternary ignimbrites of Aragats stratovolcano, western Armenia. Lithos 318, 367-382.

Gilliland, J., Austin, A., Shibesh, K., Wilmarth, M., Daskin, C., Babaya, T. 2018. Karkar, Armenia – Slimehole drilling and testing results and remote project management overview. Proceedings, 7th African Rift Geothermal Conference, Kigali, Rwanda. 31st October – 2nd November 2018.

Ghukasyan R., Meliksetian B. 1965. On the absolute age and peculiarities of formation of Meghri Pluton. Proceedings of the Academy of Sciences of the Armenian Soviet Socialist Republic, Earth Sciences Series, 18(4), 8-26.

Govindaraju, K. 1994. Compilation of working values and sample description for 383 geostandards. Geostandandards and Geoanalytical Research 18, 1-158.

Karakhanian, A., Abgaryan, Y. 2004. Evidence of historical seismicity and volcanism in the Armenian Highland (from Armenian and other sources). Annals of Geophysics 47, 793-810.

Karakhanian, A.S., Trifonov, V.G., Azizbekian, O.G., Hondkarian, D.G., 1997. Relationship of Late Quaternary tectonics and volcanism in the Khanarassar active fault zone, the Armenian Upland. Terra Nova 9, 131-134.

Karakhanian, A., Djrbashian, R., Trifonov, V., Philip, H., Arakelian, S., Avagian, A., 2002. Holocene-historical volcanism and active faults as natural risk factors for Armenia and adjacent countries. Journal of Volcanology and Geothermal Research 113, 319-344.

Karakhanian, A., Trifonov, V.G., Philip, H., Avagyan, A., Hessami, K., Jamali, F., Bayraktutan, M.S., Bagdassarian, H., Arakelian, S., Davtian, V., Adilkhanyan, A., 2004. Active faulting and natural hazards in Armenia, eastern Turkey and northwestern Iran. Tectonophysics 380, 189-219.

Karakhanian, A., Vernant, P, Doerflinger, E., Avagyan, A., Philip, H., Aslanyan, R., Champollion, C., Arakelyan, S., Collard, P., Baghdasarayn, H., Peyret, M, Davtyan, V., Calais, E., Masson, F. 2013. GPS constraints on continental deformation in the Armenian region and Lesser Caucasus. Tectonophysics 592, 39-45.

Knoll, F., Meller, H., Figur, B., Knoche, G., Schunke, T., Dresely, V., Avetisyan, P., Koiki, T., Lipták, J., Poppe, A. 2013. Die felsbilder im Hochland von Syunik. Veröffentlichungen des Landesamtes für Denkmalpflege und Archäologie Sachsen-Anhalt 67, 209-229.

Le Bas, M.J., Le Maitre, R.W., Streckeisen, A., Zanettin, B., 1986. A chemical classification of volcanic rocks based on the total alkali-silica diagram. Journal of Petrology 27, 745-750.

McDonough, W.F., Sun, S.-S., 1995. The composition of the Earth. Chemical Geology 120, 223-253.

Mederer, J., Moritz, R., Ulianov, A., Chiaradia, M., 2013. Middle Jurassic to Cenozoic evolution of arc magmatism during Neotethys subduction and arc-continent collision in the Kapan Zone, southern Armenia. Lithos 177, 61-78.

Meliksetian, Kh., 2013. Pliocene-Quaternary volcanism of the Syunik upland. Veröffentlichungen des Landesamtes für Denkmalpflege und Archäologie Sachsen-Anhalt 67, 247-258.

Meliksetian, Kh., Karakhanyan, A., Badalyan, R., Neill, I., Avagyan, A., Harutyunyan, A., Makaryan, Kh., Balasanyan, S., Navasardyan, G., Miggins, D., Koppers, A. 2018. Conference Abstract Volume; Ancient Armenia at the Crossroads, 6-7 Nov. 2018, Lyon, France, p. 12-14.

Meliksetian, Kh., Lavrushin, V., Shahinyan, H., Aidarkozhina, A., Navasardyan, G., Ermakov, A., Zakaryan, S., Prasolov, E., Maucharyan, D., Gyulnazaryan, S., Grigoryan, E. 2017. Relation of compositions of deep fluids in geothermal activity of Pleistocene-Holocene volcanic fields of Lesser Caucasus. Geophysical Research Abstracts 19, EGU2017-9674.

Messager, E., Belmecheri, S., von Grafenstein, U., Nomade, S., Ollivier, V., Voinchet, P., Puaud, S., Courtin-Nomade, A., Guillou, H., Mgeladze, A., Dumoulin, J.-P., Mazuy, A., Lordkipanidze, D. 2013. Late Quaternary record of the vegetation and catchment-related changes from Lake Paravani (Javakheti, South Caucasus). Quaternary Science Reviews 77, 125-140.

Moritz, R., Rezeau, H., Ovtcharova, M., Tayan, R.N., Melkonyan, R., Hovamkimyan, S.E., Ramazanov, V., Selby, D., Ulianov, A., Chiaradia, M., and Putlitz, B. 2016. Long-lived, stationary magmatism and pulsed porphyry systems during Tethyan subduction to post-collision evolution in the southernmost Lesser Caucasus, Armenia and Nakhitchevan. Gondwana Research 37, 465–503.

Neill, I., Meliksetian, Kh., Allen, M.B., Navasardyan, G., Karapetyan, S., 2013. Pliocene-Quaternary volcanic rocks of NW Armenia: Magmatism and lithospheric dynamics within an active orogenic plateau. Lithos 180-181, 200-215.

Neill, I., Meliksetian, Kh., Allen, M.B., Navasardyan, G., Kuiper, K., 2015. Petrogenesis of mafic collision zone magmatism: the Armenian sector of the Turkish-Iranian plateau. Chemical Geology 403, 24-41.

Niespolo EM, Rutte D, Deino AL, Renne PR, 2017. Intercalibration and age of the Alder Creek sanidine Ar-40/Ar-39 standard. Quaternary Geochronology 39, 205-213.

Nimis, P. 1999. Clinopyroxene geobarometry of magmatic rocks. Part 2. Structural geobarometers for basic to acid, tholeiitic and mildly alkaline systems. Contributions to Mineralogy and Petrology 135, 62-74.

Nimis, P. 2000. CpxBar: Clinopyroxene geobarometers for magmatic systems. Microsoft Excel spreadsheet, downloadable from: web.archive.org/web/20070727172356/http://www.dmp.unipd.it/Nimis/cpxbar3ex.zip (accessed 5/3/2019).

Ollivier, V., Nahapetyan, S., Roiron, P., Gabrielyan, I., Gasparyan, B., Chataigner, C., Joannin, S., Cornée, J.-J., Guillou, H., Scaillet, S., Munch, P., Krijgsman, W., 2010. Quaternary volcano-lacustrine patterns and palaeobotanical data in southern Armenia. Quaternary International 223, 312-326.

Pearce, J.A. (1983). Role of sub-continental lithosphere in magma genesis at active continental margins. In: Hawkesworth, C.J., Norry, M.J. (Eds) Continental Basalts and Mantle Xenoliths, Shiva Publishing, Natwich, 230-249.

Peccerillo, R., Taylor, S.R., 1976. Geochemistry of Eocene calc-alkaline volcanic rocks from the Kastamonu area, northern Turkey. Contributions to Mineralogy and Petrology 58, 63-81.

Renne, P.R., Balco G., Ludwig K.R., Mundil, R., Min, K., 2011. Response to the comment by W.H. Schwarz et al. on 'Joint determination of K-40 decay constants and the Ar-40*/K-40 for the Fish Canyon sanidine standard, and improved accuracy for Ar-40/Ar-39 geochronology" by Renne, P.R., et al., 2010. Geochimica et Cosmochimica Acta 17, 5097e5100.

Rolland, Y. 2017. Caucasus collisional history: Review of data from East Anatolia to West Iran. Gondwana Research 49, 130-146.

774 Ryan, W.B.F., Carbotte, S.M., Coplan, J.O., O'Hara, S., Melkonian, A., Arko, R., Weissel, R.A., Ferrini, V.,
775 Goodwillie, A., Nitsche, F., Bonczkowski, J., Zemsky, R. 2009. Global multi-resolution topography synthesis.
776 Geochemistry, Geophysics Geosystems 10, Q03014, doi:10.1029/2008GC002332.
777
778 Rudnick, R.L., Fountain, D.M. 1995. Nature and Composition of the Continental Crust: A Lower Crustal
779 Perspective. Reviews of Geophysics 33, 267-309.
780
781 Sahakyan, L., Bosch, D., Sosson, M., Avagyan, A., Galoyan, Gh., Rolland, Y., Bruguier, O., Stepanyan, Zh.,
782 Galland, B., Vardanyan, S. 2016. Geochemistry of the Eocene magmatic rocks from the Lesser Caucasus area
783 (Armenia): evidence of a subduction geodynamic environment. In: Sosson, M., Stephenson, R.A., Adamia, S.A.
784 (Eds.). Tectonic evolution of the eastern Black Sea and Caucasus. Geological Society of London Special
785 Publication 428, 73-98.
786
787 Sargsyan, L., Meliksetian, Kh., Metaxian, J.-P., Levonyan, A., Karakhanyan, A., Demirchyan, H., Navasardyan,
788 G., Margaryan, S., Gevorgyan, M., Babayan, H. 2017. Preliminary results of the analysis of earthquake swarms in
789 Gegham volcanic ridge (Armenia). Geophysical Research Abstracts 20, EGU2018-417.
790
791 Sosson, M., Rolland, Y., Müller, C., Danelian, T., Melkonyan, R., Kekelia, S., Adamia, A., Babazadeh, V.,
792 Kangarli, T., Avagyan, A., Galoyan, G., Mosar, J., 2010. Subductions, obduction and collision in the Lesser
793 Caucasus (Armenia, Azerbaijan, Georgia), new insights. In: Sosson, M., Kaymakci, N., Stephenson, R.A.,
794 Bergerat, F., Starostenko, V. (Eds.). Sedimentary Basin Tectonics from the Black Sea and Caucasus to the Arabian
795 Platform. Geological Society of London Special Publication 340, 329-352.
796
797 Sugden, P.J., Savov, I.P., Wilson, M., Meliksetian, K., Navasardyan, G., Halama, R. 2019. The thickness of the
798 mantle lithosphere and collision-related volcanism in the Lesser Caucasus. Journal of Petrology 60, 199-230.
799
800 Sun, S.-S., McDonough, W.F., 1989. Chemical and isotopic systematics of oceanic basalts: implications for mantle
801 composition and processes. In: Saunders, A.D., Norry, M.J. (Eds.) Magmatism in the Ocean Basins. Geological
802 Society of London Special Publication 42, 313-345.
803
804 Taylor, S.R., McLennan, S.M. 1985. The Continental Crust, Its Composition and Evolution. Blackwell, Cambridge
805 Mass., 312 pp.
806
807 White, J.T., Karakhanian, A., Connor, C.B., Connor, L., Hughes, J.D., Malservisi, R., Wetmore, P. 2015. Coupling
808 geophysical investigation with hydrothermal modelling to constrain the enthalpy classification of a potential
809 geothermal resource. Journal of Volcanology and Geothermal Research 298, 59-70.
810
811 Zobin, V.M., Gorelchik, V.I. 1982. Seismicity and source parameters of earthquakes in the region of the large
812 Tobalchik fissure eruption. Bulletin Volcanologique 45, 99-113.
813